Eur. Phys. J. D **7**, 129–135 (1999)

THE EUROPEAN PHYSICAL JOURNAL D

EDP Sciences

Electron excitation of neutral and ionic levels in Townsend discharges of argon at high E/N

G.N. Malović[1], J.V. Božin[2], B.M. Jelenković[1], and Z.Lj. Petrović[1,a]

[1] Institute of Physics, P.O.B. 57, 11001 Belgrade, Yugoslavia
[2] Faculty of Physics, University of Belgrade, P.O.Box 550, 11001 Belgrade, Yugoslavia

Received: 18 January 1999 / Received in final form: 12 April 1999

Abstract. We have measured the emission coefficients of the $3p$ levels of ArI: $3p_1$, $3p_5$, $3p_6$, $3p_7$, $3p_8$, and $3p_{10}$. The data for the $3p_5$, $3p_6$, $3p_7$, $3p_8$ and $3p_{10}$ levels were converted to excitation coefficients by using quenching coefficients from the literature. Measurements were performed in the range of E/N between $3 \times 10^{-20}\,\mathrm{Vm}^2$ to above $5 \times 10^{-18}\,\mathrm{Vm}^2$ except for the $3p_7$ level where measurements were done only up to $2 \times 10^{-19}\,\mathrm{Vm}^2$. The data for the emission coefficients for Ar II levels include two $4p'$ levels with terms $^2P^0_{1/2}$ and $^2F^0_{7/2}$, and three $4p$ levels with terms $^2P^0_{1/2}$, $^4P^0_{5/2}$ and $^2D^0_{5/2}$. The measurements for the ionic levels were done for E/N above $4 \times 10^{-19}\,\mathrm{Vm}^2$ up to nearly $1 \times 10^{-17}\,\mathrm{Vm}^2$. The absolute values of the coefficients were obtained from the intensity of the light emitted at the anode in the parallel plate self-sustained Townsend argon discharges. For low E/N the apparent emission coefficients (*i.e.* the normalized spatial profile of emission) for both neutral and ionic levels increase exponentially in almost the entire discharge gap. At about $5 \times 10^{-18}\,\mathrm{Vm}^2$ the exponentially increasing signal was obtained only near the anode, while at $1 \times 10^{-17}\,\mathrm{Vm}^2$ the spatial dependence was flat throughout the electrode gap.

PACS. 52.20.Fs Electron collisions – 52.25.Rv Emission, absorption, and scattering of visible and infrared radiation – 52.80.Dy Low-field and Townsend discharges

1 Introduction

Argon is widely used in gas discharges for plasma processing [1], and gas lasers [2]. It is often used in mixtures with other gases for reactive plasma etching [3]. Optical spectroscopy of gas discharges using Ar emission is a common nondestructive technique for obtaining information about basic processes leading to plasma applications [4]. Optical actinometry with Ar lines [5], usually the $3p^5 4p$-$3s^5 4s$ transitions ($2p$-$1s$ transitions in the Paschen notation which will be used for ArI levels in this paper), allows measurements of the density of neutral radicals in gas discharges. The actinometry based on Ar $3p$-$1s$ transitions is certainly an option when radiation from gases mixed with Ar overlaps with $2p$ transitions. The advantage of using $3p$ transitions is the smaller effect of cascading from the upper levels.

Modeling gas discharges used for plasma processing is important for testing plasma chemistry of new gas mixtures, designing plasma reactors and optimizing discharge parameters in order to improve the results of plasma processing. Results of the models have recently gained the preference of the industry to the "trial and error" approach since the cost of development has increased incredibly. The values of the excitation coefficients for $3p$ levels are important input parameters for models [6,7] and at the same time can be used as tests of models when those are applied to swarm type experiments. Excitation coefficients of $3p$ levels are required in order to be able to calculate their population density. One may also be able to determine the contribution through cascading and /or collisional quenching of $3p$ levels to the population densities of lower levels, metastables in particular. Ionic lines of argon are also often used in diagnostics of plasmas. Their advantage is that their kinetics is much simpler, with small contribution from the higher levels and collisional quenching, and the disadvantage that they can be used mainly in low-pressure plasmas with high E/N. This work is the continuation of measurements of the excitation coefficients for argon. Previously we have measured the excitation coefficients for metastables [8] and for $2p$ levels [9,10]. In this, as in the previous experiments, the excitation coefficients were obtained from the measured optical emission at the anode of the Townsend-like Ar discharge. In this paper we present absolute measurements of the electron excitation coefficients for several of the $3p$ levels of ArI and for the $^2P^0_{1/2}$, $^2F^0_{7/2}$, $^2P^0_{1/2}$, $^4P^0_{5/2}$ and $^2D^0_{5/2}$ levels of ArII.

The excitation coefficients for the $3p$ levels were obtained from the measured intensities of $3p$-$1s$ transitions. The measurements were done in the range of E/N from

[a] e-mail: zoran@Petrović.phy.bg.ac.yu

$3 \times 10^{-20}\,\mathrm{Vm}^2$ to about $5 \times 10^{-18}\,\mathrm{Vm}^2$. These measurements include the emission and excitation coefficients for the levels $3p_1$, $3p_5$, $3p_6$, $3p_7$, $3p_8$ and $3p_{10}$. The only previous data for any emission coefficient of $3p$ levels were for the $3p_5$ level by Tachibana [11]. His results were obtained at E/N from $1 \times 10^{-19}\,\mathrm{Vm}^2$ to $5 \times 10^{-19}\,\mathrm{Vm}^2$.

The coefficients for the $3p$ levels not included here were not measured due to the weakness of the available lines and/or to their overlap with other lines. If the transition from a $3p$ level overlaps with an ionic line we can still measure its excitation coefficient at lower E/N, when the excitation of the ionic level is usually too small compared to the excitation of the neutral lines. This was the case for the $3p_7$ level where we give the excitation coefficients up to $2 \times 10^{-19}\,\mathrm{Vm}^2$. The present emission (excitation) coefficients for argon ionic levels are, to our knowledge, the first measurements of this kind.

2 Experiment

Low-pressure, high-voltage Townsend discharges of Ar were sustained between two parallel disk electrodes (diameter of 79 mm), at a distance d of 17.2 mm. The anode was made of vacuum grade graphite while the cathode was made of stainless steel. The electrodes were placed in a close fitting quartz tube that enables very stable, low-current discharges on the left side of the Paschen minimum, *i.e.* the minimum of the breakdown voltage *versus* the Nd characteristics (where N is the gas number density). The same drift tube has been used for similar experiments with hydrogen [12], nitrogen [13], neon [14] and argon [9] and the details of the experimental setup can be found in these references.

Low-current discharges (typically few μA) in our drift tube can be stabilized against spontaneous current/voltage oscillations [15,16] with a large resistor (typically few MΩ) placed between the voltage power supply and the anode, and by grounding the cathode. Nevertheless, to make sure that the discharge was stable during the measurements we monitored the voltage using a fast probe and an oscilloscope. Careful design of the drift tube and of the low-capacitance electric circuit enables stable Ar discharge operation in a wide range of E/N, from $3 \times 10^{-20}\,\mathrm{Vm}^2$ to above $1 \times 10^{-17}\,\mathrm{Vm}^2$. Running discharges at currents under few μA insured uniform electric field throughout the discharge gap [17]. The dc current measurements were done using a Keithley electrometer.

The light emitted from the discharge was detected by a photomultiplier and a photon counting chain. The monochromator was used to provide a spectral resolution typically of 0.7 nm which was sufficient to integrate the line without getting any contribution of the neighbouring lines. A collimator placed between the discharge and the monochromator determined the space resolution of 0.2 mm. The monochromator and the photomultiplier were placed on a movable table driven by a stepper motor with position controlled by a computer.

The gas pressure was measured by a capacitance manometer. The pressure range covered in the experiment was between 0.1 and 15 Torr which in turn determines values of E/N ($3 \times 10^{-20}\,\mathrm{Vm}^2$ to $1 \times 10^{-17}\,\mathrm{Vm}^2$) of a self-sustained Townsend argon discharge. We have used research grade argon for the measurements. The vacuum, before the Ar was introduced into the chamber, was 3-4×10^{-7} Torr.

The calibration of the detector's quantum efficiency was done using a standard tungsten ribbon lamp. The lamp was originally calibrated against the secondary radiation standard and the details of the procedure are given in ref. [10]. The central part of the lamp's ribbon was projected onto the entrance slit of the monochomator using a quartz lens such that magnification was unity. The transmittance of the quartz window, on the vacuum chamber and on the quartz cylinder around the electrodes, was measured separately and included in the calibration.

3 Results and discussion

3.1 Data analysis

In the low-current Townsend discharges, the electrons can reach equilibrium between the energy gain from the electric field and the energy loss in the inelastic collisions with the gas atoms or molecules. The electron transport coefficients are then constant through the gap. The spatially scanned optical emission increases exponentially towards the anode since the electron number density is changing exponentially. From the exponential slope, the ionization coefficient can be determined. In view of the good agreement between the ionization coefficients obtained from the measured exponential growth of the emission and from previous measurements [18–20], we have used a fit to the exponential growth to extrapolate the signal to the anode position. The measured signal at the anode is different from the real anode signal due to effects such as the finite spatial resolution of the detector and the light reflection of the anode surface. We use the anode signal to obtain the excitation coefficients since the electron current density at the anode is equal to the measured discharge current that flows in the external ciruit. Since knowing precisely the anode position in relation to the spatial scan of the emission is important, we have tried to determine it as accurately as possible. The position of the anode was established from the separate measurements of the emission profiles of the light emitted by a pen-type light source placed behind the electrodes. Another procedure for measuring the anode position was by running the discharge under conditions such that the emission close to the anode had a sharp peak. Then the polarity of the electrodes was reversed and the position of the other electrode was measured. The distance between the electrodes, determined from emission profiles, had to agree with the known gap between the electrodes.

At high E/N and low Nd a fraction of electrons can reach the anode without reaching equilibrium. When this electron fraction starts to dominate at very high E/N, the optical emission may not increase exponentially towards

the anode. Also at high E/N, the contribution from backscattered electrons from the anode affects the growth near to the anode. These electrons consist of reflected and of secondary electrons, but the former may contribute more to the overall excitation and ionization since their energy is higher. This effect produces the emission maximum near to the anode and strongly depends on the anode material [21], so using the graphite anode reduced the effect of the backscattered electrons significantly [20]. Such processes occurring at high E/N can prevent the exponential build-up and in turn determine the upper limit for E/N in our measurements. Decreasing excitation coefficients at high E/N, particularly for neutral transitions, is another factor limiting the range of the measurements. At low E/N and high pressures we were able to run stable discharges only if the discharge currents were < 1 μA. Therefore the lower end of the E/N range is determined by the lowest discharge current that still enables stable discharges and allows measurable signal/noise ratio.

The measured intensity of the anode signal S_{mn}, due to the decay of an atom from level m to level n, normalized to the discharge current density j_e (determined at the anode), is related to the excitation coefficient ε_m/N:

$$\frac{\varepsilon_m}{N} = \frac{S_{mn}e}{K_{mn}j_eN}\frac{A_m}{A_{mn}}\left(1+\frac{N}{N_{0m}}\right),$$

here e is the electron charge, N_{0m} is the quenching density, *i.e.* the density of Ar for which half of the excited states m decay due to collisional quenching, A_m is the total transition probability of level m, A_{mn} is the transition probability of the transition $m \rightarrow n$ and $K_{mn} = \Omega VQ/4\pi$, where Ω is the effective solid angle of the detector at the axis of the discharge tube (in this experiment it was 2.5×10^3), V is the discharge volume from which the radiation was detected and Q is the quantum efficiency of the detector that includes the transmission of the quartz tube and of the monochromator. For a more detailed description of the derivation of this equation see ref. [10].

Cascading from the upper ns and nd levels can repopulate the $3p$ levels. In order to calculate the effect of the cascading contribution, it is necessary to solve coupled differential equations for the time dependence of the density of $3p$ and the high-lying s and d levels. We have done a calculation based on the experimental line intensities for $2p$ levels [9,22] and by using equations for the population and depopulation of the excited states as given in ref. [10]. We have found that the contributions vary from negligible values for $2p_1$ to nearly a factor of 2 for $2p_9$ at E/N that is greater than $2 \times 10^{-19}\,\mathrm{Vm}^2$. The $3p$ levels should be much less affected by cascading than the $2p$ ones because the levels above the $3p$ are fewer and have smaller number densities [22].

Since our technique for measuring the excitation coefficients is based on detecting the anode light after extrapolating the exponentially increasing light intensity to the anode, the uncertainty of the measurements changes with the excited level and with E/N for the same level. In general the uncertainties are smaller for lower E/N when the exponential fit can be extended almost to the cathode. Contributing to the overall uncertainty are the experimental errors in measuring the anode signal, *i.e.* anode position, errors in calibration of the detector and measurements of discharge pressure and voltage. The uncertainties in published transition probabilities and quenching coefficients need to be included as well. Our best estimate of the total uncertainty in our measurements is about 15% for the strongest lines. The weaker lines have correspondingly higher uncertainties due to a larger statistical scatter.

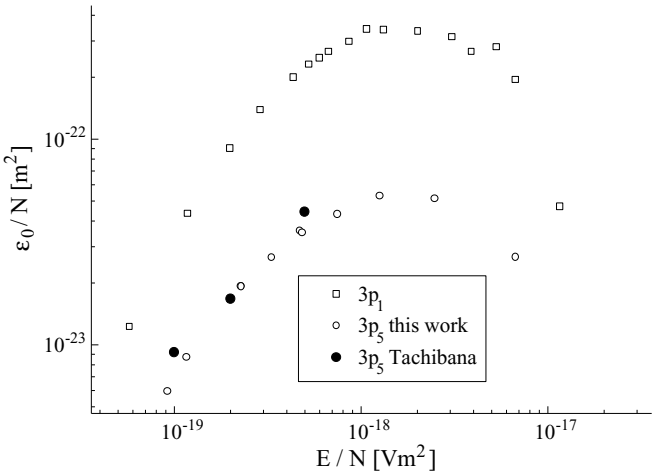

Fig. 1. Emission coefficients for $3p_1$ (open boxes) and $3p_5$ (open circles) obtained in this paper are shown as a function of E/N. Data of Tachibana [11] for $3p_5$ (solid circles) are also shown.

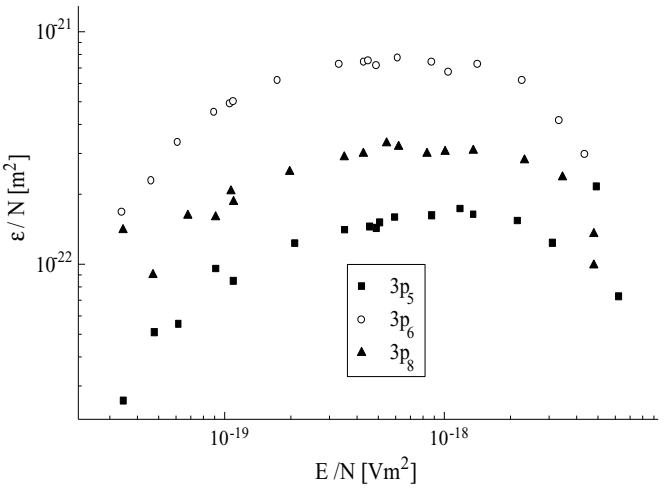

Fig. 2. Excitation coefficients for $3p_5$ (solid boxes), $3p_6$ (open circles) and $3p_8$ (solid triangles) as a function of E/N.

3.2 Excitation coefficients of the 3p levels of ArI

We have measured the emission coefficients (ε_0/N) for several $3p$ levels of ArI. These data were converted to the excitation coefficients (ε/N) by using the quenching coefficients of Inoue, Setser and Sadeghi [23]. Table 1 gives the

Table 1. Optical transitions, wavelengths, transition probabilities quenching rate coefficients used in the measurements for ArI levels.

Transition	λ (nm)	A_{ij} ($10^6\,s^{-1}$)	A_j ($10^6\,s^{-1}$)	k_q ($10^{-16}\,m^{-3}\,s^{-1}$)
$3p_1$-$1s_2$	425.9	4.15	4.15	–
$3p_5$-$1s_2$	451.07	1.23	3.99	2.7
$3p_6$-$1s_2$	415.86	1.45	1.79	3.4
$3p_7$-$1s_2$	459.61	0.1	2.17	3.7
$3p_8$-$1s_4$	430.01	0.39	0.69	3.8
$3p_{10}$-$1s_3$	452.23	0.095	0.34	5.0
$3p_{10}$-$1s_2$	470.23	0.113	0.34	5.0

Table 2. Excitation coefficients of $3p$ levels at $1 \times 10^{-19}\,Vm^2$ and $2 \times 10^{-19}\,Vm^2$.

Excited state	100 Td ε/N ($10^{-22}\,m^2$)	200 Td ε/N ($10^{-22}\,m^2$)
$3p_5$	0.848	1.23
$3p_6$	4.916	6.74
$3p_7$	9.38	11.0
$3p_8$	2.06	2.50
$3p_{10}$	13.35	22.35

optical transitions used for the measurements, their wavelengths, transition probabilities and collisional quenching rate coefficients used in the data analysis. The total quenching coefficients for the $3p$ state levels are larger than those for the $2p$ state levels as associative ionization becomes a possible channel [24,25].

The results of the excitation coefficients for the $3p$ levels at $1 \times 10^{-19}\,Vm^2$ and $2 \times 10^{-19}\,Vm^2$ are given in Table 2. In Figure 1 we show the emission coefficients for the $3p_1$ and $3p_5$ levels. For $3p_1$ we could not obtain quenching coefficients so we could not convert the data to the excitation coefficients. The data for $3p_5$ are shown here as emission coefficient values in order to make comparison with the data by Tachibana [11], who did not convert his data to excitation coefficients. Our measurements were performed under similar conditions as that of Tachibana and the agreement of the two sets of data is very good. Excitation coefficients for $3p_5$, $3p_6$ and $3p_8$ are given in Figure 2. The relative magnitude of the excitation coefficients corresponds to the relative cross-sections as measured by Lin and coworkers [26]. There are no other available data for excitation coefficients so we cannot make further comparisons. However having in mind the excellent agreement of the excitation coefficient for the $2p_1$ and $3p_5$ levels with the data of Tachibana, we may conclude that our data for the other $3p$ levels are sufficiently reliable to use in further cross-section analysis and plasma modeling.

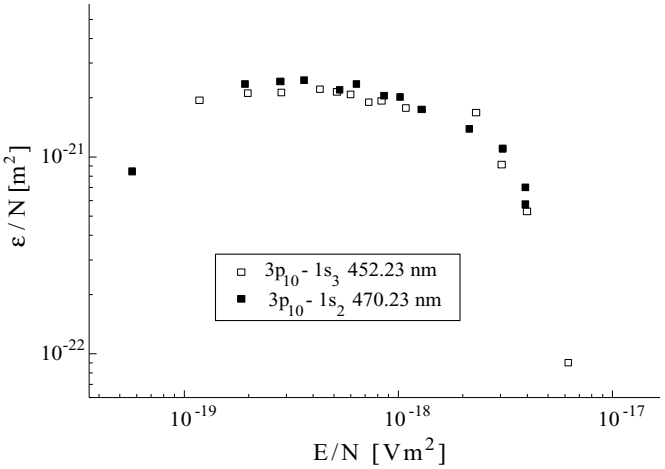

Fig. 3. Excitation coefficients for $3p_{10}$ (open triangles $3p_{10}$-$1s_3$ and solid boxes $3p_{10}$-$1s_2$) as a function of E/N.

We have also tried to measure the coefficients for $3p_{10}$. The lines that were available for the measurement were very weak, so we have used two different lines to check the internal consistency of the data. At the same time the scatter between the two sets would give limits of the accuracy of our technique obtained under the most difficult conditions, *i.e.* for the lowest signals. Two sets of data for the excitation coefficients for $3p_{10}$ were obtained using the two different transitions (see Tab. 1). The data are shown in Figure 3. The agreement between the two sets of data is very good, well within the uncertainty of the data. One should also note that in one of the preliminary presentations of the data from this paper [27] the emission coefficients were shown and were incorrectly labeled as excitation coefficients.

3.3 Excitation coefficients of the Ar II levels

We have also measured the excitation coefficients of five levels of Ar II two of the $4p'$ terms are $^2P^0_{1/2}$ and $^2F^0_{7/2}$, and three $4p$ levels terms are $^2P^0_{1/2}$, $^4P^0_{5/2}$ and $^2D^0_{5/2}$. The

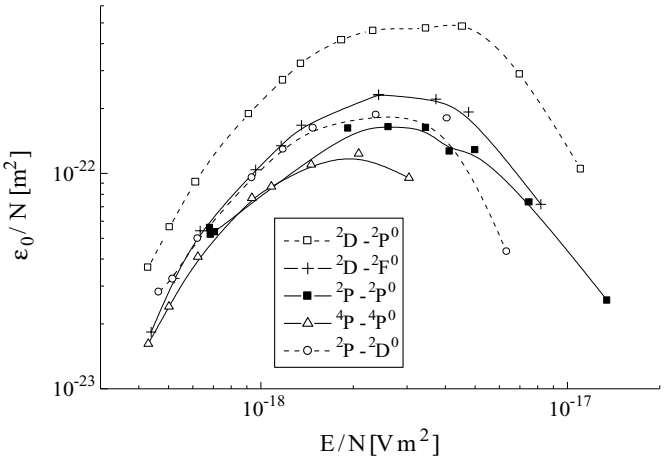

Fig. 4. Excitation coefficients for $4p\ ^2P^0_{1/2}$ (solid boxes), $4p'\ ^2F^0_{7/2}$ (crosses), $4p\ ^2P^0_{1/2}$ (open boxes), $4p\ ^4P^0_{5/2}$ (open triangles), and $4p\ ^2D^0_{5/2}$ (open points) *vs.* E/N.

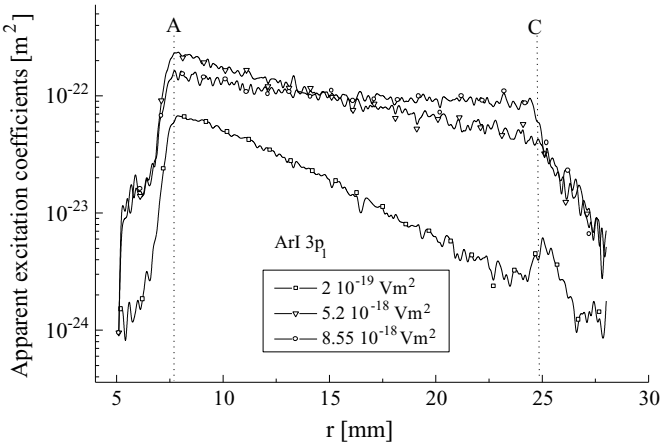

Fig. 5. Apparent excitation coefficients for the $3p_1$ level *vs.* distance between electrodes; open boxes: $2 \times 10^{-19}\,\mathrm{Vm}^2$; open triangles: $5.2 \times 10^{-18}\,\mathrm{Vm}^2$; open points: $8.55 \times 10^{-18}\,\mathrm{Vm}^2$.

Table 3. Optical transitions, wavelengths and transition probabilities used in the measurements for ArII levels.

Transition	λ (nm)	A_{ij} ($10^8\,\mathrm{s}^{-1}$)	A_i ($10^8\,\mathrm{s}^{-1}$)
$4p'\ ^2P^0_{1/2}$-$4s'\ ^2D_{3/2}$	413.17	0.85	1.802
$4p'\ ^2F^0_{7/2}$-$4s'\ ^2D_{5/2}$	460.96	0.789	1.189
$4p\ ^2P^0_{1/2}$-$4s\ ^2P_{3/2}$	465.79	0.892	1.18
$4p\ ^4P^0_{5/2}$-$4s\ ^4P_{5/2}$	480.60	0.78	1.359
$4p\ ^2D^0_{5/2}$-$4s\ ^2P_{3/2}$	487.99	0.823	1.050

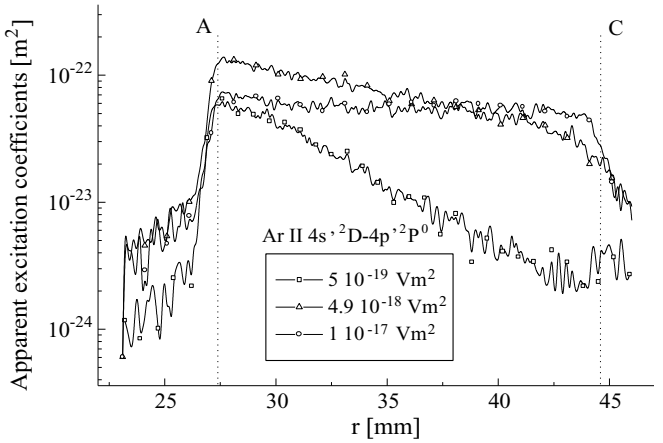

Fig. 6. Apparent excitation coefficients for the $4p'\ ^2P^0$ level *vs.* distance between electrodes; open boxes: $5 \times 10^{-19}\,\mathrm{Vm}^2$; open triangles: $4.9 \times 10^{-18}\,\mathrm{Vm}^2$; open points: $1 \times 10^{-17}\,\mathrm{Vm}^2$.

transitions used for measuring their excitation coefficients and the corresponding wavelengths are given in Table 3. The results for the excitation coefficients as a function of E/N are shown in Figure 4. We were able to extend the measurements to $8 \times 10^{-18}\,\mathrm{Vm}^2$ for the ionic lines, but there is a possibility of a development of non-equilibrium above $5 \times 10^{-18}\,\mathrm{Vm}^2$ [28]. The E/N dependences of the excitation coefficients for all the Ar II levels are similar, with peak values between 3-4$\times 10^{-18}\,\mathrm{Vm}^2$. Since the rates of collisional quenching of the ArII levels are not available in the literature, the presented results are not corrected for quenching. Assuming the coefficients to be of the order of those for the $3p$ states, and since the lifetimes of the ArII levels are very short, the quenching will not affect the data even at the highest pressures (*i.e.* the lowest E/N) used to measure the ArII excitation coefficients ($2 \times 10^{-19}\,\mathrm{Vm}^2$). Therefore we may safely regard the presented data to be equal to the excitation coefficients.

3.4 Apparent spatial excitation coefficients

In Figure 5 we show spatial profiles of emission normalized to the excitation coefficient at the anode (apparent excitation coefficients as used by Phelps and coworkers [16, 20]) for the Ar $3p_1$ level at three E/N obtained from the $3p_1$-$1s_2$ transition at 425.9 nm. The positions of the electrodes are shown by vertical dashed lines. Similar results for the $4p'^2P$-$4s\ ^2D$ level of ArII are shown in Figure 6. In each of these two figures we have included the lowest ($2 \times 10^{-19}\,\mathrm{Vm}^2$ for Ar I and $5 \times 10^{-19}\,\mathrm{Vm}^2$ for Ar II) and the highest ($8.55 \times 10^{-18}\,\mathrm{Vm}^2$ for ArI and $1 \times 10^{-17}\,\mathrm{Vm}^2$ for ArII) E/N for which the scans have been made. As can be seen from Figures 5 and 6, the exponential growth is well defined up to $5 \times 10^{-18}\,\mathrm{Vm}^2$. At higher E/N the spatial scans of emission are flat both for atomic and ionic lines. Spatial scans of optical emission are becoming flat due to the decrease of multiplication at low pressures, due to the increase of excitation close to the cathode by heavy particles [20,28] and possibly due to the onset of non-equilibrium effects for electrons [28]. In general the spatial profiles are similar to those obtained for the $2p$ levels [9,10] and consistent with the results of Phelps and

Jelenković [20] obtained at these and even higher E/N but with a longer drift tube.

4 Conclusion

In this paper we present the results for the excitation coefficients of argon using the same technique used in our previous publications, *i.e.* absolute detection of light in a Townsend discharge as a function of position and normalized at the anode. Results for $3p$ levels of Ar I and for $4p$ and $4p'$ levels of ArII are shown here. We were not able to measure the excitation coefficients as a function of E/N for all $3p$ levels due to the overlapping lines of argon in the region between 300 and 450 nm. Emission and excitation coefficients were obtained for a wide range of E/N, from $3 \times 10^{-20}\,\mathrm{Vm}^2$ to about $5 \times 10^{-18}\,\mathrm{Vm}^2$, for 5 lines, $3p_1$, $3p_5$, $3p_6$, $3p_8$ and $3p_{10}$ and up to $2 \times 10^{-19}\,\mathrm{Vm}^2$ for $3p_7$. With the exception of the $3p_5$ level the measurements were presented for the first time in the literature. Tachibana's results for $3p_5$ [11] obtained for $E/N < 5 \times 10^{-19}\,\mathrm{Vm}^2$ are in good agreement with our results. The E/N dependence of the excitation coefficients is similar for all the levels, and the absolute magnitudes are in agreement with the relative magnitudes of the cross-sections.

The excitation coefficients for the ionic levels are reported for the first time in the literature. We needed a discharge with E/N of at least $4 \times 10^{-19}\,\mathrm{Vm}^2$ to be able to measure those excitation coefficients. The measurements include two $4p'$ levels ($^2P^0_{1/2}$ and $^2F^0_{7/2}$), and three $4p$ levels ($^2P^0_{1/2}$, $^4P^0_{5/2}$, $^2D^0_{5/2}$). The measured excitation coefficients have a very similar dependence as a function of E/N, increasing up to $2 \times 10^{-18}\,\mathrm{Vm}^2$ followed by a flat region to about $5 \times 10^{-18}\,\mathrm{Vm}^2$. The few points that we have measured beyond $5 \times 10^{-18}\,\mathrm{Vm}^2$ indicate that the excitation coefficients are decreasing with E/N.

The spatial variations of the optical emission for both neutral and ionic transitions at different E/N were given in terms of spatial apparent excitation coefficients. The spatial dependence varies from the exponential throughout most of the discharge gap at low E/N to nearly flat at high E/N. The spatial scans flatten due to a combined effects of low electron multiplications, possible electron non-equilibrium behavior and heavy particle excitation. Data for neutral $3p$ level at $E/N \leq 8 \times 10^{-18}\,\mathrm{Vm}^2$ show that emission begins to increase near to the cathode, presumably due to the excitation by fast neutral Ar. By comparing the spatial apparent excitation coefficients for $3p$ with $2p$ data, reported earlier [9,10,20,28], the heavy particle excitation appears to dominate the excitation of $2p$ levels near to the cathode at lower E/N.

The measured spatial excitation coefficients at high E/N are a useful test of models and Monte Carlo simulations. The excitation coefficients are also useful in the normalization of the electron excitation cross sections and in putting the emission diagnostic of gas discharges on the absolute scale. We hope that the present data may be of use in the diagnostics of plasmas for etching [29], sputtering [30] and gas lasers.

We acknowledge the partial financial support by the MNTRS 01E03 Project. We would like to thank Dr. A.V. Phelps for careful reading of the manuscript, numerous suggestions and support.

List of Symbols

E/N: reduced electric field [Vm^2];

ε_m/N: excitation coefficient [m^2];

S_{mn}: measured intensity of the signal at the anode, for level m to level n transition;

j_e: current density;

e: electron charge;

N_{0m}: quenching density;

A_m: the total transition probability of the level m;

A_{mn}: transition probability of the transition $m \rightarrow n$;

Ω: effective solid angle of the detector at the axis of the discharge tube;

V: discharge volume from which the radiation is detected;

Q: quantum efficiency.

References

1. H.F. Winters, J. Vac. Sci. Technol. A **6**, 1997 (1988); A. J. van Roosmalen, Vacuum **34**, 429 (1984); U. Gerlach-Meyer, J.W. Coburn, E. Kay, Surf. Sci. **103**, 177 (1981); D.J. Oostra, A. Haring, A.E. de Vries, J. Vac. Sci. Technol. B **4**, 1278 (1986).
2. C.K. Rhodes, *Excimer Lasers* (Springer Verlag, Berlin, 1979).
3. M.J. Kushner, W.Z. Collison, M.J. Grapperhaus, J.P. Holland, M.S. Barnes, J. Appl. Phys. **80**, 1337 (1996).
4. K. Rozsa, A. Gallagher, Z. Donko, Phys. Rev. E **52**, 913 (1995).
5. J.W. Coburn, M. Chen, J. Vac. Sci. Technol. **18**, 353 (1981); S.E. Savas, Appl. Phys. Lett. **48**, 1042 (1986); S. Radovanov, B. Tomčik, Z.Lj. Petrović, B. M. Jelenković, J. Appl. Phys. **67**, 97 (1990).
6. A. Bogaerts, R. Gijbels, J. Appl. Phys. **78**, 6427 (1995).
7. Z.Lj. Petrović, S. Bzenić, J. Jovanović, S. Durović, J. Phys. D **28**, 2287 (1995).
8. J.V. Božin, V.V. Urošević, Z.Lj. Petrović, Z. Phys. A **312**, 349 (1983).
9. Z.M. Jelenak, Z.B. Velikić, J.V. Božin, Z.Lj. Petrović, B.M. Jelenković, Phys. Rev. E **47**, 3566 (1993).
10. J. V. Božin, Z.M. Jelenak, Z.V. Velikić, I.D. Belca, Z.Lj. Petrović, B.M. Jelenković, Phys. Rev. E **53**, 52 (1996).
11. K. Tachibana, Phys. Rev. A **34**, 1007 (1986).
12. Z. Stokić, M.M.F.R. Fraga, J.V. Božin, V. Stojanović, Z.Lj. Petrović, B.M. Jelenković, Phys. Rev. A **45**, 7463 (1992).
13. V. Stojanović, J. V. Božin, Z.Lj. Petrović, B. M. Jelenković, Phys. Rev. A **42**, 4983 (1990).
14. G.N. Malović, J.V. Božin, B.M. Jelenković, Z.Lj. Petrović, Nucl. Inst. Meth. B **129**, 317 (1997).
15. Z.Lj. Petrović, A.V. Phelps, Phys. Rev. E **47**, 2806 (1993).
16. A.V. Phelps, Z. Lj. Petrović, B.M. Jelenković, Phys. Rev. E **47**, 2825 (1993).
17. Z.Lj. Petrović, A.V. Phelps, Phys. Rev. E **56**, 5920 (1998).
18. A.A. Kruithof, Physica (Utrecht) **7**, 519 (1940).

19. C.S. Lakshimnarasimha, J. Lucas, J. Phys. D **10**, 313 (1977).
20. A.V. Phelps, B.M. Jelenković, Phys. Rev. A **38**, 2975 (1988).
21. M.E. Woods, B.J. Hopkins, G.F. Matthews, G.M. McCraken, P.M. Sewell, H. Fahrang, J. Phys. D **20**, 1136 (1987).
22. Z.Lj. Petrović, J.V. Jovanović, Z.M. Raspopović, S.A. Bzenić, S.B. Vrhovac, Aust. J. Phys. **50**, 591 (1997); Z.Lj. Petrović, J. Jovanović, S. Vrhovac, J.T. Broad, *XVI Summer School and International Symposium on the Physics of Ionized Gases*, edited by M. Milosavljević (Institute of nuclear Science, Vinča, Belgrade, 1993), p. 66; F. Tochikubo, Z.Lj. Petrović, S. Kakuta, N. Nakano, T. Makabe, Jpn J. Appl. Phys. **33**, 4271 (1994).
23. G. Inoue, D.W. Setser, N. Sadeghi, J. Chem. Phys. **76**, 977 (1982).
24. V. Puech, L. Torchin, J. Phys. D **19**, 2309 (1986).
25. B.M. Smirnov, Sov. Phys. Usp. **24**, 251 (1981).
26. J.E. Chilton, J.B. Boffard, R.S. Schappe, C.C. Lin, Phys. Rev. A **57**, 267 (1998).
27. G. Malović, J. Božin, B.M. Jelenković, Z.Lj. Petrović, *Proc. XXIII International Conference on ionized gases*, edited by M.C. Bordage, A. Gleizes (Université Paul Sabatier, Toulouse, 1997), pp. I-98.
28. Z.Lj. Petrović, V.D. Stojanović, J. Vac. Sci. Technol. A **16**, 329 (1998).
29. A. Okigawa, T. Makabe, Z.Lj. Petrović, T. Shibagaki, T. Kogawa, A. Itoh, Jpn J. Appl. Phys. **35**, 1890 (1996).
30. T. Tokonami, T. Makabe, Appl. Phys. Lett. **72**, 3323 (1992).